

# Optimization of relativistic mean field model for finite nuclei to neutron star matter

B. K. Agrawal<sup>1</sup>, and A. Sulaksono<sup>2</sup> and P. -G. Reinhard<sup>3</sup>

<sup>1</sup>*Saha Institute of Nuclear Physics, Kolkata - 700064, India.*

<sup>2</sup>*Departemen Fisika, FMIPA, Universitas Indonesia, Depok, 16424, Indonesia.*

<sup>3</sup>*Institut für Theoretische Physik II, Universität Erlangen-Nürnberg,  
Staudtstrasse 7, D-91058 Erlangen, Germany.*

## Abstract

We have optimized the parameters of extended relativistic mean-field model using a selected set of global observables which includes binding energies and charge radii for nuclei along several isotopic and isotonic chains and the iso-scalar giant monopole resonance energies for the  $^{90}\text{Zr}$  and  $^{208}\text{Pb}$  nuclei. The model parameters are further constrained by the available informations on the energy per neutron for the dilute neutron matter and bounds on the equations of state of the symmetric and asymmetric nuclear matter at supra-nuclear densities. Two new parameter sets BSP and IUFSU\* are obtained, later one being the variant of recently proposed IUFSU parameter set. The BSP parametrization uses the contributions from the quartic order cross-coupling between  $\omega$  and  $\sigma$  mesons to model the high density behaviour of the equation of state instead of the  $\omega$  meson self-coupling as in the case of IUFSU\* or IUFSU. Our parameter sets yield appreciable improvements in the binding energy systematics and the equation of state for the dilute neutron matter. The importance of the quartic order  $\omega - \sigma$  cross coupling term of the extended RMF model, as often ignored, is realized.

PACS numbers: 21.10.-k, 21.65+f, 24.30.Cz, 21.60.jz, 26.60.+c

## I. INTRODUCTION

The concept of effective field theory has provided a modern perspective to the relativistic mean-field (RMF) models [1, 2]. The extended RMF models, motivated by the basic ideas of effective field theory, are obtained by expanding the energy density functional in powers of the fields for scalar-isoscalar ( $\sigma$ ), vector-isoscalar ( $\omega$ ) and vector-isovector ( $\rho$ ) mesons and their derivatives upto a given order  $\nu$ . The extended RMF model thus includes the contributions from all possible self and cross coupling interaction terms for  $\sigma$ ,  $\omega$  and  $\rho$  mesons in addition to the cubic and quartic self interaction terms for  $\sigma$  meson as present in the conventional quantum hydrodynamic based relativistic mean field models [3, 4]. The parameters (or the expansion coefficients) appearing in the energy density functional of the extended RMF model are so adjusted that the resulting set of nuclear observables agree well with the corresponding experimental data. The extended RMF models containing terms upto the quartic order ( $\nu = 4$ ) can be satisfactorily applied to study the properties of finite nuclei. Inclusion of next higher order terms improves the fit to the finite nuclear properties only marginally. Even high density behaviour of the equation of state (EOS) of nucleonic matter is predominantly controlled by the quartic order  $\omega$  meson self-coupling [5]. The effects of higher order terms on the high density behaviour of EOS are found to be only modest to negligible. We would like to mention that the density dependent meson exchange [6–9] and density dependent point coupling [10] versions of the RMF models are also very successful in describing the ground state properties of the finite nuclei.

There have been several parameterizations [2, 11–15] of extended RMF models. Earlier parameter sets G1, G2 and TM1\* were generated by considering almost all the terms upto the quartic order. These parameterizations yield strong linear density dependence of the symmetry energy coefficient and the nuclear matter incompressibility coefficient is either little too low or quite high. Later, FSU parameterization [16, 17] demonstrated that the linear density dependence of the symmetry energy and the nuclear matter incompressibility coefficient can be reasonably obtained simply by appropriately adjusting the strengths of the  $\omega - \rho$  cross-coupling and the  $\omega$  meson self-coupling terms of the extended RMF model. For the FSU parameters, the limiting mass of the neutron star is only  $1.7M_{\odot}$  which is somewhat smaller than the currently proposed limit of  $2M_{\odot}$  [18]. The value of the limiting mass of neutron stars could be significantly increased by changing  $\omega$  meson self-coupling strength

within a reasonable range [5]. In Refs. [19, 20], we have shown that the strength of  $\omega$  meson self-coupling can be varied in such a way that the limiting mass of the neutron stars ranges from  $1.7 - 2.4M_{\odot}$ , and still bulk properties of the finite nuclei and nuclear matter at saturation density remain practically unaffected.

Recently, IUFSU parameter set [21] of the extended RMF model is obtained by readjusting the strength of the  $\omega - \rho$  cross-coupling and  $\omega$  meson self-coupling in such a way that the neutron skin of  $^{208}\text{Pb}$  nucleus is 0.16 fm and limiting neutron star mass is  $\sim 2.0M_{\odot}$ . The remaining parameters of the model, instead of fitting to the bulk properties of the finite nuclei, were tuned to yield the properties of the nuclear matter at the saturation density which are very much close to those for the FSU parameters. The EOSs for the symmetric nuclear matter (SNM) and the pure neutron matter (PNM) obtained for the IUFSU parameters, in the density range  $2.5 - 4.5\rho_0$  ( $\rho_0 = 0.16 \text{ fm}^{-3}$ ), agree reasonably with the ones extracted by analyzing the heavy-ion collisions data. However, energy per neutron for the PNM at sub nuclear densities seems somewhat larger in comparison to those obtained from the various microscopic approaches. The EOS for the  $\beta$ -equilibrated neutron rich matter at high densities is softer than those deduced from the neutron star observables. The FSU or IUFSU like parametrizations do not include the contributions from the  $\omega - \sigma$  cross-coupling terms. The presences of these terms might improve the high density behaviour of the EOS of the nucleonic matter. Nevertheless, influence of such cross-coupling on the high density behaviour of EOS for the nucleonic matter remain largely unexplored.

The objective of present work is twofold. We would like to optimize the extended RMF model using a large set of experimental data on binding energies and charge radii instead of those for just a few closed shell nuclei as normally done. Our data set consists of the binding energies and charge radii for the nuclei along several isotopic and isotonic chains. The values of the constrained energies for the isoscalar giant monopole resonance (ISGMR) for the  $^{90}\text{Zr}$  and  $^{208}\text{Pb}$  nuclei are also considered in our fit. Further, the model parameters are constrained by available informations on the energy per neutron for the dilute neutron matter and bounds on the EOSs for the SNM, PNM and the  $\beta$ -equilibrated neutron rich matter at supra-nuclear densities. Another objective of the present work is to investigate whether the inclusion of  $\omega - \sigma$  cross-coupling can improve the situation encountered by FSU or IUFSU like parameterizations.

The paper is organized as follows. The extended RMF model is outlined briefly in Sec. II.

The fit observables and the constraints employed to optimize the extended RMF model are discussed in Sec. III. In Sec. IV we present two newly generated parameter sets and several bulk properties for the symmetric nuclear matter at saturation density. In Sec. V we discuss our results for the EOSs for the nuclear and neutron star matters and compare them with those for few existing parameterization of the extended RMF model. The results for the bulk properties of finite nuclei and neutron stars obtained using our newly generated parameter sets are presented in Secs. VI and VII. Finally, summary and out look are presented in Sec. VIII.

## II. THE EXTENDED RMF MODEL

The derivations of the effective Lagrangian density and corresponding energy density functionals for the extended RMF model are well documented in Refs. [1, 2, 12]. The effective Lagrangian density used in the present work can be written as [2, 5],

$$\mathcal{L} = \mathcal{L}_{\mathcal{NM}} + \mathcal{L}_\sigma + \mathcal{L}_\omega + \mathcal{L}_\rho + \mathcal{L}_{\sigma\omega\rho}. \quad (1)$$

where the Lagrangian  $\mathcal{L}_{\mathcal{NM}}$  describing the interactions of the nucleons through the mesons is,

$$\mathcal{L}_{\mathcal{NM}} = \sum_{J=n,p} \bar{\Psi}_J [i\gamma^\mu \partial_\mu - (M - g_\sigma \sigma) - (g_\omega \gamma^\mu \omega_\mu + \frac{1}{2} g_\rho \gamma^\mu \tau \cdot \rho_\mu)] \Psi. \quad (2)$$

Here, the sum is taken over the neutrons and protons and  $\tau$  are the isospin matrices. The Lagrangian describing self interactions for  $\sigma$ ,  $\omega$ , and  $\rho$  mesons can be written as,

$$\mathcal{L}_\sigma = \frac{1}{2} (\partial_\mu \sigma \partial^\mu \sigma - m_\sigma^2 \sigma^2) - \frac{\kappa_3}{6M} g_\sigma m_\sigma^2 \sigma^3 - \frac{\kappa_4}{24M^2} g_\sigma^2 m_\sigma^2 \sigma^4, \quad (3)$$

$$\mathcal{L}_\omega = -\frac{1}{4} \omega_{\mu\nu} \omega^{\mu\nu} + \frac{1}{2} m_\omega^2 \omega_\mu \omega^\mu + \frac{1}{24} \zeta_0 g_\omega^2 (\omega_\mu \omega^\mu)^2, \quad (4)$$

$$\mathcal{L}_\rho = -\frac{1}{4} \rho_{\mu\nu} \rho^{\mu\nu} + \frac{1}{2} m_\rho^2 \rho_\mu \rho^\mu. \quad (5)$$

The  $\omega^{\mu\nu}$ ,  $\rho^{\mu\nu}$  are field tensors corresponding to the  $\omega$  and  $\rho$  mesons, and can be defined as  $\omega^{\mu\nu} = \partial^\mu \omega^\nu - \partial^\nu \omega^\mu$  and  $\rho^{\mu\nu} = \partial^\mu \rho^\nu - \partial^\nu \rho^\mu$ . The cross interactions of  $\sigma$ ,  $\omega$ , and  $\rho$  mesons are described by  $\mathcal{L}_{\sigma\omega\rho}$  which can be written as,

$$\begin{aligned} \mathcal{L}_{\sigma\omega\rho} = & \frac{\eta_1}{2M} g_\sigma m_\omega^2 \sigma \omega_\mu \omega^\mu + \frac{\eta_2}{4M^2} g_\sigma^2 m_\omega^2 \sigma^2 \omega_\mu \omega^\mu + \frac{\eta_\rho}{2M} g_\sigma m_\rho^2 \sigma \rho_\mu \rho^\mu \\ & + \frac{\eta_{1\rho}}{4M^2} g_\sigma^2 m_\rho^2 \sigma^2 \rho_\mu \rho^\mu + \frac{\eta_{2\rho}}{4M^2} g_\omega^2 m_\rho^2 \omega_\mu \omega^\mu \rho_\mu \rho^\mu. \end{aligned} \quad (6)$$

One also needs to include the contributions from the electromagnetic interaction in the case of finite nuclei. The Lagrangian density  $\mathcal{L}_{em}$  for the electromagnetic interaction can be written as,

$$\mathcal{L}_{em} = -\frac{1}{4}F_{\mu\nu}F^{\mu\nu} - e\bar{\Psi}_p\gamma_\mu A_\mu\Psi_p, \quad (7)$$

where,  $A$  is the photon field and  $F^{\mu\nu} = \partial^\mu A^\nu - \partial^\nu A^\mu$ . The equation of motion for nucleons, mesons and photons can be derived from the Lagrangian density defined in Eq.(1). The contributions from Eq. (7) are included only for the case of finite nuclei.

It can be seen that there are five cross-coupling terms in Eq. (6). Two of them are the cubic order terms of the  $\omega - \sigma$  and  $\sigma - \rho$  cross-couplings and three quartic order terms corresponding to the  $\omega - \sigma$ ,  $\sigma - \rho$  and  $\omega - \rho$  cross-couplings. The cross-coupling terms involving  $\rho$ -meson field enables one to vary the density dependence of the symmetry energy coefficient and the neutron skin thickness in heavy nuclei over a wide range without affecting the other properties of finite nuclei [20, 22, 23]. The contribution from the  $\omega - \sigma$  cross-couplings and self coupling of  $\omega$ -mesons play important role in varying the high density behaviour of the EOSs and also prevents instabilities in them [5, 11, 13]. It may be noted from Eq. (5) that the contributions of the self-coupling of  $\rho$  mesons are not considered. Because, expectation value of the  $\rho$ -meson field is order of magnitude smaller than that for the  $\omega$ -meson field [2]. Thus, inclusion of the  $\rho$ -meson self interaction can affect the properties of the finite nuclei and neutron stars only very marginally [5].

We would like to briefly outline the manner in which the corrections to the binding energies arising from the center of mass motion, pairing and quadrupole correlations are incorporated. The spurious center of mass energy  $E_{cm}$  is evaluated as [24],

$$E_{cm} = -17.2 A^{-0.2} \text{ MeV}. \quad (8)$$

The above estimate for the  $E_{cm}$  is obtained by fitting the the full center of mass correction calculated microscopically for several nuclei. We include the corrections to the binding energy due to the pairing correlations when the nucleon numbers are non-magic. The contributions from the pairing correlations are evaluated in the constant gap approximation with the gap [25],

$$\Delta = \frac{11.2}{\sqrt{A}} \text{ MeV}. \quad (9)$$

The pairing correlation energies for a fixed gap  $\Delta$  is calculated using the pairing window of  $2\hbar\omega = 82A^{-1/3} \text{ MeV}$ . Soft nuclei and deformed nuclei can develop substantial contributions

from quadrupole correlations [26]. We use a simple estimate for the quadrupole correlation energy or rotational correction as,

$$E_{\text{rot}} = 2.2\sqrt{\beta_2 - 0.05} m/m^* \text{ MeV} \quad (10)$$

where  $\beta_2$  is the nuclear quadrupole deformation and  $m^*$  is the nucleon effective mass in bulk equilibrium matter. This estimate has been extracted by studying the microscopically computed trends of  $E_{\text{rot}}$  for a wide variety of Skyrme-Hartree-Fock parameterizations [27]. The rotation corrections are included only for the nuclei with  $\beta_2 > 0.05$ . The Eq. (10) is not relevant for the fitted nuclei as all of them are spherical. But, we shall need it for the binding energy systematics which is obtained by calculating the binding energies for known even-even nuclei and some of them are well deformed. To this end, we may point out that the contributions from the Coulomb exchange terms are ignored.

### III. FIT OBSERVABLES AND SOME CONSTRAINTS

The parameters for most of the conventional and extended RMF models are obtained by fitting the binding energies and charge rms radii only for few closed shell nuclei [12, 13, 16, 28, 29]. We fit the parameters of the extended RMF model to the experimental data for the binding energy, charge rms radius and energy for ISGMR. We use the binding energies for 62 nuclei and charge radii for 50 nuclei as listed in the Tables I and II. These nuclei lie along several isotopic and isotonic chains. The errors on the binding energies and charge rms radii used for the chi-square minimization are also given in these tables. The same set of nuclei are used in Ref. [30] to obtain a set of systematically varied Skyrme forces. The experimental data for the ISGMR constrained energies included in our fit are 17.81 MeV for the  $^{90}\text{Zr}$  nucleus and 14.18 MeV for the  $^{208}\text{Pb}$  nucleus [31] with the theoretical error taken to be 0.2 MeV. We also constrain the model parameters, using some available informations on the EOS for the nuclear and neutron star matter at supra-nuclear densities together with energy per neutron for the dilute neutron matter.

The EOSs for the SNM and the PNM are available in terms of the pressure versus density [32]. We considered 6 data points for each of these EOSs over the density range  $\rho = 2.0 - 4.5\rho_0$ . The EOS for the  $\beta$ -equilibrated neutron rich matter are available in terms of pressure versus energy density [33]. We consider 32 data points for this EOS for the

energy density ranging from  $150 - 1600 \text{ MeV} fm^{-3}$ . The theoretical error on the pressure is taken to be 25% of its required value. The realistic EOSs for the dilute neutron matter are available in terms of the energy per neutron versus neutron density [34]. For this case we take 8 data points over the range of neutron density  $\rho_n = 0.1 - 0.3\rho_0$ . The theoretical errors used for the energy per neutron is 0.05 MeV.

#### IV. NEW PARAMETRIZATIONS AND NUCLEAR MATTER PROPERTIES

We have obtained two different parameter sets of the extended RMF model. We name them as 'BSP' and 'IUFSU\*', later one being the variant of recently proposed IUFSU parameter set. The name BSP for one of our parameter set is derived from the initials of the authors of the present work. The parameter set BSP includes contributions from  $\omega - \sigma$  and  $\omega - \rho$  cross-couplings. The parameter set IUFSU\* includes the contributions from  $\omega$  meson self-coupling and  $\omega - \rho$  cross-coupling. In other words, the high density behaviour of the EOS for the parameter set BSP is governed by the quartic order  $\omega - \sigma$  cross-coupling. Whereas, in case of the IUFSU\* it is governed by the  $\omega$  meson self-coupling. For the IUFSU\* set, the strength  $\zeta_0$  for the  $\omega$  meson self-coupling is such that  $\zeta_0/g_\omega^2 = 0.03$  same as that for the IUFSU parameterization. This value of  $\zeta_0$  yields optimum behaviour for the EOSs of the SNM, PNM and neutron star matter at high densities. Similarly, for the BSP parameterization, the value of  $\eta_2$  is adjusted to optimize the EOSs for the nuclear and neutron star matter at high densities. The strength  $\eta_{2\rho}$  of the  $\omega - \rho$  cross-coupling (Eq. (6)) is adjusted to yield reasonable agreement with the energy per neutron for the dilute neutron matter for both the BSP and IUFSU\* parameter sets. The remaining parameters of the model are obtained by fitting the binding energies and charge rms radii of the nuclei as listed in Tables I and II. The best fit parameters are searched using the simulated annealing method which has been applied to determine the parameters of the extended RMF model and Skyrme type effective forces [19, 35, 36]. In Table III, we list the values for the newly generated parameter sets. We have given the values for the G1, G2, TM1\* and NL3 parameter sets. They will be used to compute the EOSs for the infinite nuclear matter and the neutron star matter for the comparison with those obtained for the newly generated parameter sets. It must be pointed out that some of the coupling parameters of the parameter sets BSP, IUFSU\* and IUFSU are quite different from the unity or equivalently they show significant deviations

from the naturalness. This is clearly due to the fact that not all the terms upto the quartic order are considered. So, the reduction in the number of the parameters is possible only at the cost of their naturalness.

In Table IV we list the values of various quantities associated with nuclear matter calculated at the saturation density. These quantities are evaluated as follows,

$$K = 9\rho^2 \frac{d^2 E(\rho, 0)}{d\rho^2}, \quad (11)$$

$$E_{\text{sym}} = \frac{1}{2} \left. \frac{d^2 E(\rho, \delta)}{d\delta^2} \right|_{\delta=0}, \quad (12)$$

$$L = 3\rho \frac{dE_{\text{sym}}}{d\rho}, \quad (13)$$

$$K_{\text{asy}} = K_{\text{sym}} - 6L, \quad (14)$$

$$K_{\text{sat},2} = K_{\text{asy}} - \frac{Q}{K}L, \quad (15)$$

$$K_{\text{sym}} = 9\rho^2 \frac{d^2 E_{\text{sym}}}{d\rho^2}, \quad (16)$$

$$Q = 27\rho^3 \frac{d^3 E(\rho, 0)}{d\rho^3} \quad (17)$$

where,  $E(\rho, \delta)$  is the energy per nucleon at a given density  $\rho$  and asymmetry  $\delta = (\rho_n - \rho_p)/\rho$ . The incompressibility coefficient  $K$  together with  $K_{\text{sat},2}$  at the saturation density can yield the value of incompressibility coefficient for asymmetric nuclear matter [37]. One can use the values of  $E_{\text{sym}}$ ,  $L$  and  $K_{\text{sym}}$  at the saturation density to evaluate the density dependence of the symmetry energy coefficient which in turn can yield the EOS for asymmetric nuclear matter [37]. It can be seen from Table IV that values of  $E_{\text{sym}}$  and  $L$  are quite high for the G1, G2, TM1\* and NL3 parameterizations in comparison to those for BSP, IUFSU\* and IUFSU parameter sets.

## V. EQUATIONS OF STATE

We now compare our results for the EOSs for SNM, PNM and  $\beta$ -equilibrated neutron rich matter with those obtained for a few existing parameterizations of the extended RMF model. As a customary we also compare our results with those for the NL3 parameter set of the conventional RMF model which includes non-linear terms only for the  $\sigma$ -mesons. It may be instructive to first look into the density dependence of the symmetry energy coefficient  $E_{\text{sym}}$  and its slope  $L$  as they play predominant role in understanding the behaviour of the

EOSs for the PNM and the beta equilibrated neutron rich matter. In Figs. 1 and 2 we plot the density dependence of  $E_{\text{sym}}$  and its slope  $L$  for various parameterizations of the extended RMF model as listed in Table III. The inset in Fig. 1 highlights the behaviour of  $E_{\text{sym}}$  at sub-nuclear densities. The G1, G2, TM1\* and NL3 parameterizations yield stiffer symmetry energy at supra-nuclear densities. Whereas, at densities  $\rho < 0.1 \text{ fm}^{-3}$ , these parameter sets yield softer symmetry energy. We find that  $E_{\text{sym}} = 30.0, 30.9$  and  $31.8$  MeV and  $L = 53.9, 53.9$  and  $49.2$  MeV at  $\rho_0$  for the BSP, IUFSU\* and IUFSU parameter sets, respectively. These values are reasonably well within  $E_{\text{sym}} = 30.5 \pm 3.0$  MeV and  $L = 52.5 \pm 20$  MeV as estimated recently by confronting the Skyrme Hartree-Fock results [38] with several empirical constraints. We would like to add that the values of  $E_{\text{sym}}$  and  $L$  for the BSP, IUFSU\* and IUFSU parameter sets are also in close agreement with the ones extracted from the experimental data on the iso-vector giant dipole resonance [39, 40].

In Fig. 3 we plot the energy per neutron for the PNM at low densities. We compare these results with those calculated using various microscopic approaches [34]. The energy per neutron for the PNM for G1, G2, TM1\* and NL3 parameterizations is smaller at low densities in comparison to those obtained from various microscopic approaches. While, IUFSU yield higher values for energy per neutron for the PNM at sub-nuclear densities. Our parameterizations, namely, BSP and IUFSU\* yield reasonable values for the energy per neutron at low densities for the PNM. These parametrizations include EOS corresponding to  $\text{HF} - V_{\text{lowk}(SP)}$  of Fig. 3 into the fit. The low density behaviour of the energy per neutron can be easily understood from the inset of Fig. 1. For instance, the softer symmetry energy coefficient for the G1 parameter set at sub-nuclear densities is responsible for lower values for the energy per neutron. In Figs. 4 and 5 we plot the EOSs for the SNM and PNM respectively in terms of pressure versus nucleon density, . The bounds on the EOSs as shown by shaded regions are the ones extracted by analyzing the heavy-ion collision data [32]. Clearly, EOSs for the BSP, IUFSU\* and IUFSU parameterizations are in better agreement with the ones shown by shaded region. The EOS for SNM for the G2 set is also quite reasonable, but, it yields relatively stiffer EOS for the PNM. Thus, it appears from the various EOSs plotted in Figs. 3 - 5 that the overall performance of BSP, IUFSU\* and IUFSU parameter sets are somewhat better relative to the other parameter sets considered.

In Fig. 6, EOSs for the beta equilibrated neutron rich matter are plotted in terms of pressure versus energy density. Various bounds on the EOSs as depicted by shaded regions

are extracted by the neutron star observables [33]. The orange and the black boundaries of the shaded regions are the EOSs within  $1\sigma$  and  $2\sigma$  limits, respectively. It appears at first glance that, except for the NL3 parameter set, all the other parameterizations yield similar trends for the EOS of the beta equilibrated neutron rich matter. Most of the EOSs calculated using extended RMF model lie within  $1\sigma$  limit for the energy densities approximately 500 – 700 MeV/fm<sup>3</sup>. Only the EOS corresponding to the BSP parameterization stays either within or very close to its  $1\sigma$  limit up to very high energy densities. In fact, if we consider only the best performers, i.e., BSP, IUFSU\* and IUFSU parameterizations, it can be seen that at very high energy densities  $\epsilon \geq 900$  MeV/fm<sup>3</sup>, the EOSs for IUFSU\* and IUFSU tend to go below the  $1\sigma$  limit EOS and eventually crosses  $2\sigma$  limit. We may recall that the high density behaviour for the BSP parametrization is governed by the quartic order  $\omega - \sigma$  cross-coupling, whereas, for the IUFSU\* parametrizations it is governed by the  $\omega$ -meson self-coupling. Thus, the improvement in the high density behaviour of the EOS for the BSP parameter set is indicative of the importance of the contributions of the quartic order  $\omega - \sigma$  cross-coupling.

## VI. FINITE NUCLEI

We have computed some bulk properties of finite nuclei using the BSP, IUFSU\* and IUFSU parameter sets of the extended RMF model. The binding energies for 513 known even-even nuclei are calculated to get the binding energy systematics. In Fig. 7 we display our results for the binding energy systematics in terms of errors  $\delta B$  given as,

$$\delta B = B_{\text{th}} - B_{\text{exp}} \quad (18)$$

where,  $B_{\text{th}}$  and  $B_{\text{exp}}$  are the theoretical and experimental values for the binding energy. We have indicated the present state of the art by  $\pm 1$  MeV error bars. The binding energy is better described in case of BSP and IUFSU\* in comparison to that for the IUFSU case. We calculate the rms error for the binding energies using the results for all the 513 even-even nuclei as considered in the present work. These rms errors as given in the parenthesis in the units of MeV are: BSP (2.7), IUFSU\*(2.6) and IUFSU (5.7). It is to be noted that the rms error on the binding energy for our newly generated parameter sets BSP and IUFSU\* are smaller by more than twice in comparison to that for the IUFSU. We would like to emphasize,

this significant improvement is obviously due to the fact that we have optimized our model using the bulk properties of the large number of finite nuclei, unlike, the IUFSU parameters as discussed in Sec. I. In Ref. [27], we presented the binding energy systematics for the BSR4 parameter set of the extended RMF model in which almost all the terms present in Eq. (6) were included. The rms error on the binding energy for the BSR4 parameter set is 2.6 MeV. This indicates that the terms ignored in the present work might have only small bearing on our results. To be more precise, the terms ignored in the present work at best could improve only the naturalness of the parameters. We do not show our results for the charge radii, since, their values for the BSP, IUFSU\* and IUFSU parametrizations are very much similar. The rms error for the charge radii calculated using the nuclei considered in the fits is  $\sim 0.02$  fm for all the three cases.

We calculate the constraint energy  $E_{\text{con}}$  for the ISGMR as,

$$E_{\text{con}} = \sqrt{\frac{m_1}{m_{-1}}} \quad (19)$$

where,  $m_1$  and  $m_{-1}$  are the energy and inverse energy weighted moments of the ISGMR strength function. The fully self-consistent and highly accurate values for  $m_1$  and  $m_{-1}$  are calculated for non-relativistic mean-field models in Ref. [41]. We follow similar strategy to evaluate  $m_1$  and  $m_{-1}$ . Once the mean-field equations are solved, the  $m_1$  can be expressed in terms of the ground state density  $\rho$  as,

$$m_1 = 2 \frac{\hbar^2}{M} \langle r^2 \rangle, \quad (20)$$

where,

$$\langle r^2 \rangle = \int r^2 \rho(r) d\mathbf{r}. \quad (21)$$

The moment  $m_{-1}$  can be evaluated via constrained RMF approach and is given as,

$$m_{-1} = \left. \frac{1}{2} \frac{d}{d\lambda} \langle r_\lambda^2 \rangle \right|_{\lambda=0} \quad (22)$$

where,  $\langle r_\lambda^2 \rangle$  is calculated using Eq. (21), but, the density  $\rho(r)$  is now obtained from the solutions of the constrained single-particle Hamiltonian  $H_\lambda = H - \lambda r^2$ . We have compared our values of the  $E_{\text{con}}$  for  $^{208}\text{Pb}$  nucleus for the NL3 and FSU forces with those obtained within the RPA approach [42]. The values of  $E_{\text{con}}$  for both of these approaches differ at most by 0.04 MeV. The values of  $E_{\text{con}}$  for several nuclei are compared with corresponding

experimental data in Fig. 8. The overall trends for  $E_{\text{con}}$  for all the three parameter sets of the extended RMF model as considered are quite similar.

The neutron skin,  $R_n - R_p$ , the difference between the rms radii for the point neutrons and protons density distributions, is calculated using BSP, IUFSU\* and IUFSU parameter sets. In Fig. 9, the values of  $R_n - R_p$  for the several tin isotopes are compared with the corresponding experimental data [39, 43–47]. The values of neutron-skin thickness for the  $^{208}\text{Pb}$  nucleus are 0.153, 0.164 and 0.161 fm for the BSP, IUFSU\* and IUFSU parameter sets, respectively. Our values of neutron-skin for  $^{208}\text{Pb}$  nucleus are in harmony with the  $0.158^{+0.025}_{-0.02}$  fm deduced very recently from the correlations of the dipole polarizability and the neutron-skin [48, 49] as well as with  $0.175 \pm 0.02$  fm as estimated using the Skyrme Hartree Fock results [50].

## VII. NEUTRON STARS

The mass-radius relation of neutron star is important to understand the high density behavior of hadronic EOS. To this end, some static neutron star properties are calculated by solving Tolman Oppenheimer Volkov (TOV) equation. The outer crust region of the neutron star is described using the EOS of R  ster *et al.* [51]. This EOS is the recent update of the one given by Baym, Pethick, and Sutherland [52]. Due to the fact that the detailed EOS of inner crust indeed is not yet certain, the polytrophic pressure-energy density relation is used to interpolate the EOS for the region between outer crust and the core [21]. The core is assumed to be composed of either the nucleonic or the hyperonic matter in  $\beta$ -equilibrium. The EOS of the core is obtained from the different parameter sets of the extended RMF model as discussed in Sec. IV. The meson-hyperon coupling constants as required to compute the hyperonic EOS are taken from Refs. [20, 53, 54]. In Fig. 10 the mass-radius relations predicted by IUFSU, IUFSU\* and BSP parameter sets are plotted using their nucleonic and hyperonic EOSs. For comparison we also show the observational constraints extracted from the analysis of Refs.[33, 55] as well as the recent larger pulsar mass observed [18].

In the case of nucleonic EOS, the BSP and IUFSU\* parameter sets predict slightly larger maximum mass compared to the ones of IUFSU. However, the BSP parameter set yields the radius  $R_{1.4}$  for the neutron star with the canonical mass ( $1.4M_\odot$ ) which lies in between

those for the IUFSU\* and IUFSU sets. The maximum mass predicted by each parameter set is in the range of the constraint region predicted by larger pulsar mass observation [18]. BSP and IUFSU\* predictions still also touch the upper part of  $2\sigma$  region extracted from the analysis of Steiner *et al.* [33]. While the threshold density for the direct URCA process and its corresponding mass  $M_{\text{DU}}$  as well as the transition density from core to inner crust and its corresponding pressure predicted by BSP and IUFSU\* parameter sets are quite close to the ones predicted by IUFSU (see Table V).

The hyperonic star properties predicted by BSP are quite similar to the ones of IUFSU\* except that the BSP parameter set predicts relatively smaller maximum mass radius compared to that of IUFSU\*. On the other hand by comparing the particle fraction of BSP (right panel) and IUFSU\* (left panel) of Fig. 11, it can be seen that they have similar pattern, only the  $\Sigma^0$  of BSP appears rather earlier i.e., at  $\rho_B \sim 9\rho_0$  then that of IUFSU\* i.e., at  $\rho_B \sim 10\rho_0$ . Thus beside difference in nonlinear term used in both parameter sets which is discussed in previous section, the difference in the number of  $\Sigma^0$  predicted by both parameter sets might also influence maximum mass radius predictions. The mass-radius relationship as obtained using the nucleonic EOSs of the core are in better agreement with the region extracted from the analysis of Steiner *et al.* [33]. However, the maximum mass predicted by both parameter sets are still too small compared to the mass of pulsar J1614-2230. The effects of the presence of hyperons in maximum mass and Direct Urca mass predictions of both parameter sets can be seen in Table V.

## VIII. SUMMARY AND OUTLOOK

We have optimized the extended RMF model using a large set of experimental data for the bulk properties of finite nuclei. The nuclear bulk properties included in the fit are the binding energies and charge radii of the nuclei along several isotopic and isotonic chains and the ISGMR energies for the  $^{90}\text{Zr}$  and  $^{208}\text{Pb}$  nuclei. The density dependence of the symmetry energy coefficient is constrained by energy per neutron for the dilute neutron matter calculated in a microscopic approach. The model parameters are further constrained by the observational bounds on the EOS of SNM, PNM, and beta equilibrated neutron rich matter at supra-nuclear densities. Two different parameter sets named BSP and IUFSU\* are obtained. Later one being the variant of recently proposed IUFSU parameter set. The

main difference between the BSP and the IUFSU\* is that, in case of BSP the high density behaviour of the EOS is controlled by  $\omega - \sigma$  quartic order cross-coupling and in case of the IUFSU\* it is governed by the  $\omega$  meson self-coupling. We see significant improvement in the binding energy systematics (Fig. 7) and the energy per neutron for the dilute neutron matter (Fig. 3) over those for the IUFSU parameter set. The EOS for the beta equilibrated matter for the BSP parameter set (Fig. 5) lie within or very close to its  $1\sigma$  limit bounds extracted using neutron star observables. These EOSs for the cases of IUFSU\* and IUFSU show somewhat larger deviations. In particular, the pressure at higher energy densities ( $\epsilon > 900$  MeV/fm<sup>3</sup>) tend to become increasingly lower than the lower bound of the  $1\sigma$  limit so much so that it eventually crosses the  $2\sigma$  limit. This difference in the high density behaviour of the EOSs for the BSP and IUFSU\* indicates importance of the contributions of the quartic order  $\omega - \sigma$  cross-coupling, as often ignored.

We find that the BSP and IUFSU\* yield the symmetry energy coefficient  $E_{\text{sym}} = 31$  MeV and its slope  $L = 54$  MeV and the neutron-skin for the <sup>208</sup>Pb nucleus is 0.15–0.16 fm. These values are in good agreement with the ones determined by confronting the Skyrme Hartree-Fock results to various empirical constraints [38, 49, 50]. The neutron star properties of BSP and IUFSU\* parameter sets using nucleonic EOS for the neutron star core are quite similar with the ones predicted by IUFSU. However, if hyperons are included, the BSP predict smaller maximum mass radius compared to the one of IUFSU\*.

The present work demonstrates that the contributions of quartic order  $\omega - \sigma$  cross-couplings are important in order to model the high density behaviour of the EOS. The predictability of the extended RMF model may be still improved by including the contributions from the several gradient terms for the meson fields as presently ignored. These terms would contribute only for the finite nuclei allowing one to adjust simultaneously the properties of the finite nuclei and the infinite matter. Further, we would like to point out that in the present work we do not include the contributions from the  $\delta$  mesons which are important in order to explain the splitting of proton and neutron effective masses [56]. The  $\delta$  meson also influences the high density behaviour of the asymmetric nuclear matter. The work along this lines is underway.

- 
- [1] R. Furnstahl, B. D. Serot, and H.-B. Tang, Nucl. Phys. **A598**, 539 (1996).
  - [2] B. D. Serot and J. D. Walecka, Int. J. Mod. Phys. E **6**, 515 (1997).
  - [3] J. D. Walecka, Ann. Phys. (N.Y.) **83**, 491 (1974).
  - [4] J. Boguta and A. R. Bodmer, Nucl. Phys. **A292**, 413 (1977).
  - [5] H. Müller and B. D. Serot, Nucl. Phys. **A606**, 508 (1996).
  - [6] S. Typel and H. Wolter, Nucl. Phys. **A656**, 331 (1999).
  - [7] T. Niksic, D. Vretenar, P. Finelli, and P. Ring, Phys. Rev. C **66**, 024306 (2002).
  - [8] W. Long, J. Meng, N. V. Giai, and S.-G. Zhou, Phys. Rev. C **69**, 034319 (2004).
  - [9] G. A. Lalazissis, T. Niksic, D. Vretenar, and P. Ring, Phys. Rev. C **71**, 024312 (2005).
  - [10] T. Niksic, D. Vretenar, and P. Ring, Phys. Rev. C **78**, 034318 (2008).
  - [11] Y. Sugahara and H. Toki, Nucl. Phys. **A579**, 557 (1994).
  - [12] R. Furnstahl, B. D. Serot, and H.-B. Tang, Nucl. Phys. **A615**, 441 (1997).
  - [13] M. D. Estal, M. Centelles, X. Vias, and S. K. Patra, Phys. Rev. C **63**, 024314 (2001).
  - [14] S. Gmuca and J. K. Bunta, Nucl. Phys. A **734**, 172 (2004).
  - [15] S. Gmuca, Acta. Phys. Hungarica A **19**, 155 (2004).
  - [16] B. G. Todd-Rutel and J. Piekarewicz, Phys. Rev. Lett **95**, 122501 (2005).
  - [17] J. Piekarewicz and S. P. Weppner, nucl-th/0509019 (2005).
  - [18] P. B. Demorest, T. Pennucci, S. M. Ransom, M. S. E. Roberts, and J. W. T. Hessels, Nature **467**, 1081 (2010).
  - [19] R. Kumar, B. K. Agrawal, and S. K. Dhiman, Phys. Rev. C **74**, 034323 (2006).
  - [20] S. K. Dhiman, R. Kumar, and B. K. Agrawal, Phys. Rev. C **76**, 045801 (2007).
  - [21] F.J.Fattoyev, C.J.Horowitz, J/Piekarewicz, and G.Shen, Phys. Rev. C **82**, 055803 (2010).
  - [22] R. Furnstahl, Nucl. Phys. **A706**, 85 (2002).
  - [23] T. Sil, M. Centelles, X. Vinas, and J. Piekarewicz, Phys. Rev. **C71**, 045502 (2005).
  - [24] J. Friedrich and P.-G. Reinhard, Phys. Rev. C **33**, 335 (1986).
  - [25] P. Ring and P. Schuck, The nuclear many-body problems (Springer, New York-Heidelberg-Berlin, 1980).
  - [26] P. Klüpfel, J. Erler, P.-G. Reinhard, and J. A. Maruhn, Eur. Phys. J. A **37**, 343 (2008).
  - [27] P. G. Reinhard and B. K. Agrawal, Int. J. Mod. Phys. E **20**, 1379 (2011).

- [28] G. A. Lalazissis, J. König, and P. Ring, Phys. Rev. C **55**, 540 (1997).
- [29] B. D. Serot and J. D. Walecka, Adv. Nucl. Phys. **16**, 1 (1986).
- [30] P. Klüpfel, P.-G. Reinhard, T. J. Burvenich, and J. A. Maruhn, Phys. Rev. C **79**, 034310 (2009).
- [31] D. H. Youngblood, H. L. Clark, and Y. W. Lui, Phys. Rev. Lett. **82**, 691 (1999).
- [32] P. Danielewicz, W. G. Lynch, and R. Lacey, Science **298**, 1592 (2002).
- [33] A.W.Steiner, J.M.Lattimer, and E.F.Brown, Astrophysics J. **722**, 33 (2010).
- [34] A. Gezerlis and J. Carlson, Phys. Rev. C **81**, 025803 (2010).
- [35] B. K. Agrawal, S. Shlomo, and V. K. Au, Phys. Rev. C **72**, 014310 (2005).
- [36] B. K. Agrawal, S. K. Dhiman, and R. Kumar, Phys. Rev. C **73**, 034319 (2006).
- [37] L.-W. Chen, B.-J. Cai, C. M. Ko, B.-A. Li, C. Shen, and J. Xu, Phys. Rev. C **80**, 014322 (2009).
- [38] L.-W. Chen, Phys. Rev. C **83**, 044308 (2011).
- [39] A. Klimkiewicz and et al., Phys. Rev. C **76**, 051603 (2007).
- [40] A. Carbone, G. Colo, A. Bracco, L.-G. Cao, P. F. Bortignon, F. Camera, and O. Wieland, Phys. Rev. C **81**, 041301 (2010).
- [41] O. Bohigas, A. M. Lane, and J. Martorell, Phys. Rep. **51**, 267 (1979).
- [42] J. Piekarewicz, private communications (????).
- [43] L. Ray, Phys. Rev. C **19**, 1855 (1979).
- [44] A. Krasznahorkay, A. Balanda, J. A. Bordewijk, S. Brandenburg, M. N. Harakeh, B. M. N. Kalantar-Nayestanaki, J. Timr, and A. van der Woude, Nucl. Phys. A **567**, 521 (1994).
- [45] A. K. et al., Phys. Rev. Lett. **82**, 3216 (1999).
- [46] A. Trzcinska, J. Jastrzebski, P. Lubinski, F. J. Hartmann, R. Schmidt, T. von Egidy, and B. Klos, Phys. Rev. Lett. **87**, 082501 (2001).
- [47] S. Terashima and et al., Phys. Rev. C **77**, 024317 (2008).
- [48] P.-G. Reinhard and W. Nazarewicz, Phys. Rev. C **81**, 051303 (2010).
- [49] A. Tamii and *et al*, Phys. Rev. Lett. **107**, 062502 (2011).
- [50] L.-W. Chen, C. M. Ko, B.-A. Li, and J. Xu, Phys. Rev. C **82**, 024321 (2010).
- [51] S. B. Ruster, M. Hampel, and Schaffner-Bielich, Phys. Rev. C **73**, 035804 (2006).
- [52] G. Baym, C. Pethick, and P. Sutherland, Astrophys. J. **170**, 299 (1971).
- [53] J. Schaffner-Bielich and A. Gal, Phys. Rev. C **62**, 034311 (2000).

- [54] C. Ishizuka, A. Ohnishi, K. Tsubakihara, K. Sumiyoshi, and S. Yamada, J. Phys. G **35**, 085201 (1996).
- [55] F. Ozel, G. Baym, and T. Guver, Phys. Rev. D **82**, 101301 (2010).
- [56] X. Roca-Maza, X.Vinas, M. Centelles, P. Ring, and P. Schuck, Phys. Rev. C **84**, 054309 (2011).
- [57] J. Carriere, C. Horowitz, and J. Piekarewicz, Astrophys. J. **593**, 463 (2003).

TABLE I: Experimental data for the binding energies  $E_B$  and charge rms radii  $r_{rms}$  used in the fits (part I: along isotopic chain). The second line shows the globally adopted error for each observable. That error is multiplied for each observable by a further integer weight factor which is given in the column next to the data value.

A	Z	$E_B$		$r_{rms}$	
		$\pm 1$ MeV		$\pm 0.02$ fm	
16	8	-127.620	4	2.701	2
36	20	-281.360	2	3.478 3.513 3.523 3.502 3.479 3.523	1 2 2 1 2 9
38	20	-313.122	2		
40	20	-342.051	3		
42	20	-361.895	2		
44	20	-380.960	2		
46	20	-398.769	2		
48	20	-415.990	1		
50	20	-427.491	1		
52	20	-436.571			
56	28	-483.990	5	3.750	9
58	28	-506.500	5	3.776	5
60	28	-526.842	5	3.818	5
62	28	-545.258	5	3.848	5
64	28	-561.755	5	3.868	5
68	28	-590.430			

Table I continued.

100	50	-825.800	2		
108	50			4.563	2
112	50			4.596	9
114	50			4.610	9
116	50			4.626	9
118	50			4.640	1
120	50			4.652	1
122	50	-1035.530	3	4.663	1
124	50	-1050.000	3	4.674	1
126	50	-1063.890	2		
128	50	-1077.350	2		
130	50	-1090.400	1		
132	50	-1102.900	1		
134	50	-1109.080	1		
198	82	-1560.020	9	5.450	2
200	82	-1576.370	9	5.459	1
202	82	-1592.203	9	5.474	1
204	82	-1607.521	2	5.483	1
206	82	-1622.340	1	5.494	1
208	82	-1636.446	1	5.504	1
210	82	-1645.567	1	5.523	1
212	82	-1654.525	1	5.542	1
214	82	-1663.299	1	5.559	1

TABLE II: Experimental data for the fits, (part II: along isotonic chains). Doubly magic nuclei which would fit both sequences are not repeated here. For further explanations see table I.

A	Z	$E_B$		$r_{\text{rms}}$	
		$\pm 1 \text{ MeV}$		$\pm 0.02 \text{ fm}$	
34	14	-283.429	2		
36	16	-308.714	2	3.299	1
38	18	-327.343	2	3.404	1
42	22	-346.904	2		
50	22	-437.780	2	3.570	1
52	24	-456.345		3.642	2
54	26	-471.758		3.693	2
84	34	-727.341			
86	36	-749.235	2	4.184	1
88	38	-768.467	1	4.220	1
90	40	-783.893	1	4.269	1
92	42	-796.508	1	4.315	1
94	44	-806.849	2		
96	46	-815.034	2		
98	48	-821.064	2		
134	52	-1123.270	1		
136	54	-1141.880	1	4.791	1
138	56	-1158.300	1	4.834	1
140	58	-1172.70	1	4.87	1
142	60	-1185.150	2	4.915	1
144	62	-1195.740	2	4.96	1
146	64	-1204.440	2	4.984	1
148	66	-1210.750	2	5.046	2
150	68	-1215.330	2	5.076	2
152	70	-1218.390	2		
206	80	-1621.060	1	5.485	1
210	84	-1645.230	1	5.534	1
212	86	-1652.510	1	5.555	1
214	88	-1658.330	1	5.571	1

TABLE III: Various parameter sets for the extended RMF model. All the parameters are dimensionless. The nucleon mass  $M$  is 939.2 MeV for the BSP and IUFSU\*, 939.0 MeV for G1,G2 [12], NL3 [28] and IUFSU [21] and 938 MeV for TM1\* [13].

	BSP	IUFSU*	IUFSU	G1	G2	TM1*	NL3
$g_\sigma/4\pi$	0.8764	0.8379	0.7935	0.7853	0.8352	0.8930	0.8131
$g_\omega/4\pi$	1.1481	1.0666	1.0371	0.9651	1.0156	1.1920	1.0240
$g_\rho/4\pi$	1.0508	0.9889	1.0815	0.6984	0.7547	0.7960	0.7121
$\kappa_3$	1.0681	1.1418	1.3066	2.2067	3.2467	2.5130	1.4661
$\kappa_4$	14.9857	1.0328	0.1074	-10.0900	0.6315	8.9700	-5.6718
$\eta_1$	0.0872	0.0	0.0	0.0706	0.6499	1.10	0.0
$\eta_2$	3.1265	0.0	0.0	-0.9616	0.1098	0.10	0.0
$\eta_\rho$	0.0	0.0	0.0	-0.2722	0.3901	0.4500	0.0
$\eta_{1\rho}$	0.0	0.0	0.0	0.0	0.0	0.0	0.0
$\eta_{2\rho}$	53.7642	41.3066	51.4681	0.0	0.0	0.0	0.0
$\zeta_0$	0.0	5.3895	5.0951	3.5249	2.6416	3.60	0.0
$m_\sigma/M$	0.5383	0.5430	0.5234	0.5396	0.5541	0.5450	0.5412
$m_\omega/M$	0.8333	0.8331	0.8333	0.8328	0.8328	0.8348	0.8333
$m_\rho/M$	0.8200	0.8198	0.8216	0.8200	0.8200	0.8209	0.8126

TABLE IV: Some bulk properties of the nuclear matter at the saturation density ( $\rho_s$ ): binding energy per nucleon ( $B/A$ ), incompressibility coefficient for symmetric nuclear matter ( $K$ ), symmetry energy ( $E_{\text{sym}}$ ), linear density dependence of the symmetry energy ( $L$ ) and various quantities ( $K_{\text{sym}}$ ), ( $K_{\text{asy}}$ ) and ( $K_{\text{sat2}}$ ) as given by Eqs. (11-15).

Force	$B/A$ (MeV)	$\rho_s$ (fm $^{-3}$ )	$K$ (MeV)	$E_{\text{sym}}$ (MeV)	$L$ (MeV)	$K_{\text{sym}}$ (MeV)	$K_{\text{asy}}$ (MeV)	$K_{\text{sat2}}$ (MeV)
BSP	15.9	0.149	230	28.83	50	9	-290	-218
IUFSU*	16.1	0.150	236	29.85	50	12	-289	-234
IUFSU	16.4	0.155	231	31.30	47	28	-254	-195
G1	16.1	0.153	215	38.5	123	96	-642	-434
G2	16.1	0.153	215	36.4	100	-7	-611	-404
TM1*	16.3	0.145	281	37	102	-14	-625	-429
NL3	16.3	0.148	272	37.4	118	100	-608	-700

TABLE V: Tabulation of some neutron star observables in the case of without and with (+H) hyperons.  $M^{\text{max}}$  is the maximum mass,  $R_{\text{min}}$  is its radius.  $R_{1.4}$  is the radius of  $1.4 M_{\odot}$  where  $M_{\odot}$  is solar mass.  $\rho_{\text{DU}}$  is the threshold density for the direct URCA process,  $M_{\text{DU}}$  is the minimum neutron star's mass that may cool down by the direct URCA process.  $\rho_t$  is the transition density [57] from core to inner crust of neutron star and  $P_t$  is the pressure at  $\rho_t$ .

	IUFSU [21]	IUFSU*	BSP	IUFSU*+H	BSP+H
$M^{\text{max}}/M_{\odot}$	1.94	1.96	2.02	1.53	1.54
$R_{\text{min}}$ (km)	11.19	11.40	11.03	11.65	10.32
$R_{1.4}$ (km)	12.49	12.81	12.64	12.79	12.58
$\rho_{\text{DU}}$ (fm $^{-3}$ )	0.61	0.61	0.60	0.59	0.60
$M_{\text{DU}}/M_{\odot}$	1.77	1.81	1.82	1.48	1.45
$\rho_t$ (fm $^{-3}$ )	0.087	0.081	0.087	0.081	0.087
$P_t$ (MeVfm $^{-3}$ )	0.28	0.30	0.29	0.30	0.29

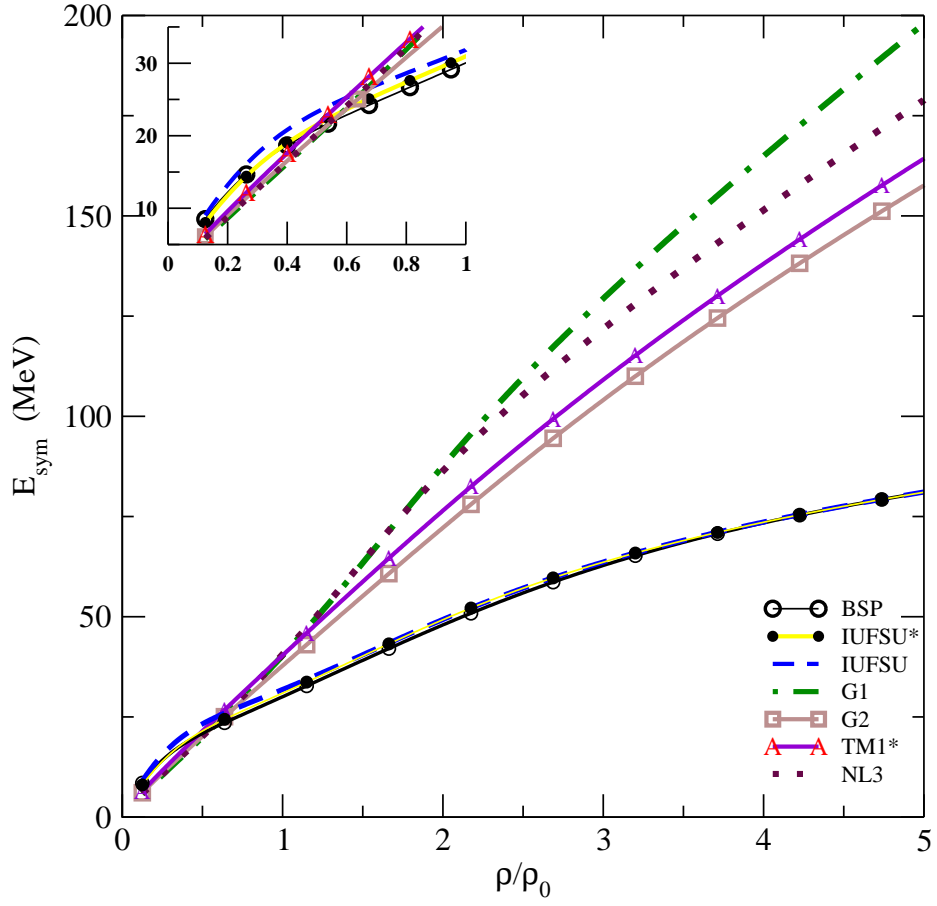


FIG. 1: (Color online) The symmetry energy coefficient  $E_{\text{sym}}$  plotted as a function of density  $\rho/\rho_0$  ( $\rho_0 = 0.16 \text{ fm}^{-3}$ ) for several parameterizations of the extended RMF model. The inset highlights the behaviour of  $E_{\text{sym}}$  at sub-nuclear densities.

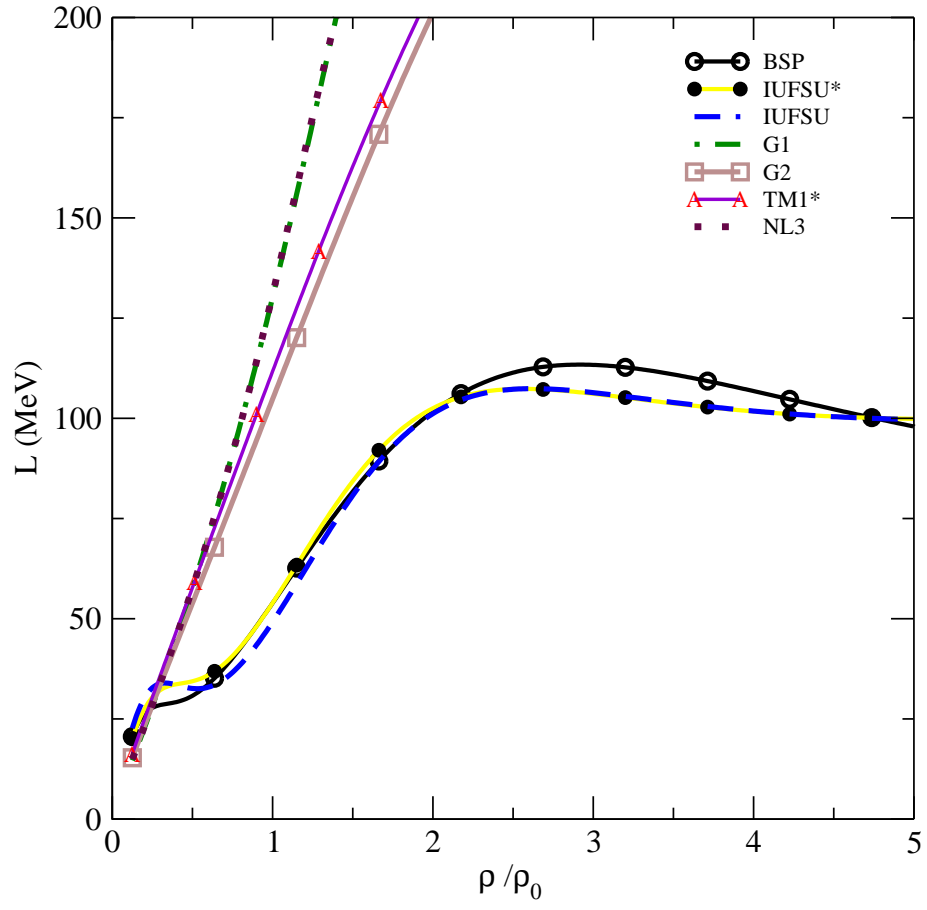


FIG. 2: (Color online) Plots for the slope,  $L$ , of symmetry energy coefficient as a function of density for several parameterizations of the extended RMF model.

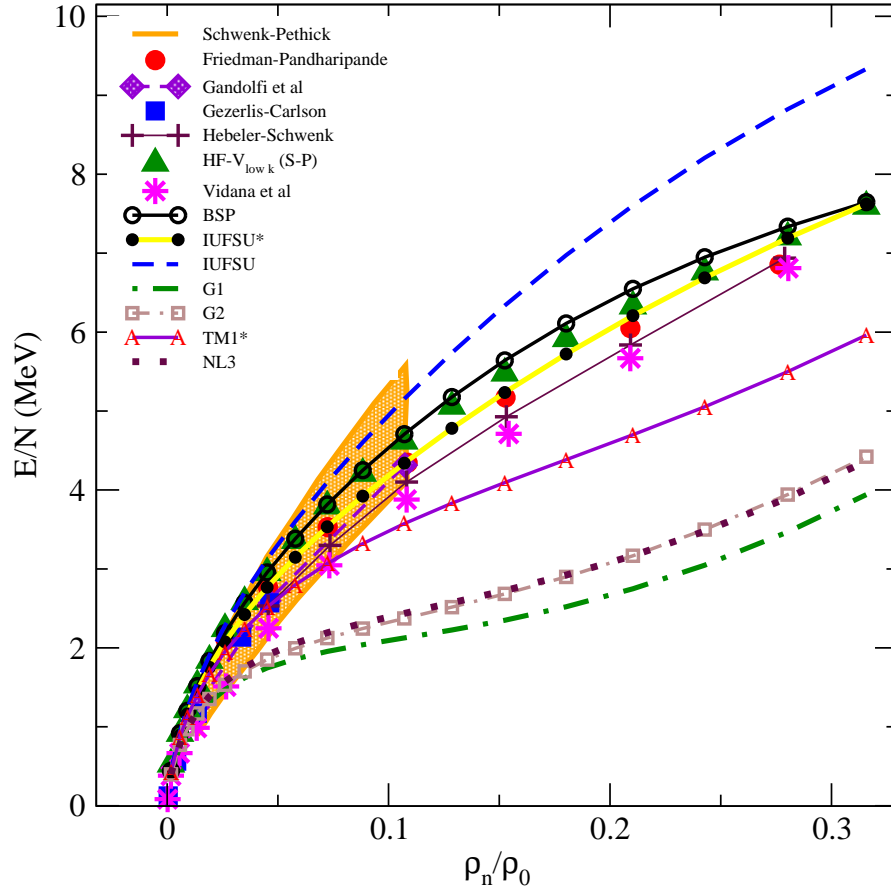


FIG. 3: (Color online) Plots for energy per neutron as a function of neutron density. The curves labeled BSP, IUFSU\*, IUFSU, G1, G2, TM1\* and NL3 denote various parameter sets for the extended RMF model. Other curves represent the results for various microscopic approaches [34].

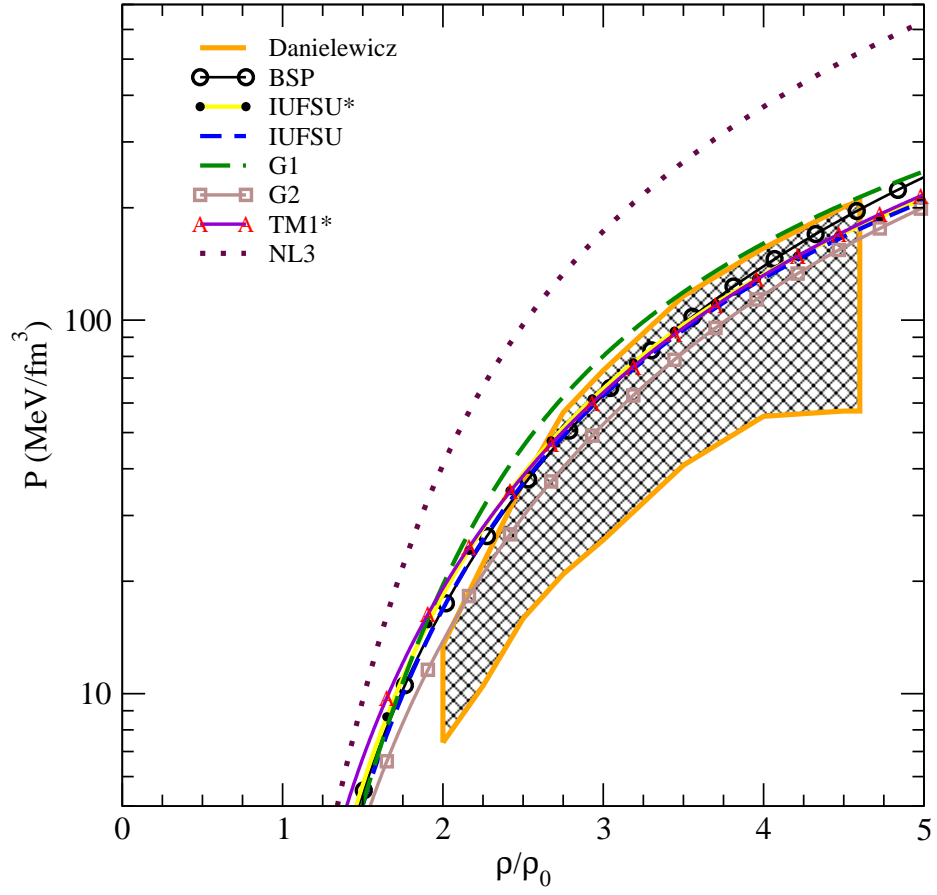


FIG. 4: (Color online) Pressure as a function of nucleon density for the SNM. The shaded area represents the EOS extracted from the analysis of Ref. [32]. The density is scaled by  $\rho_0 = 0.16 \text{ fm}^{-3}$ .

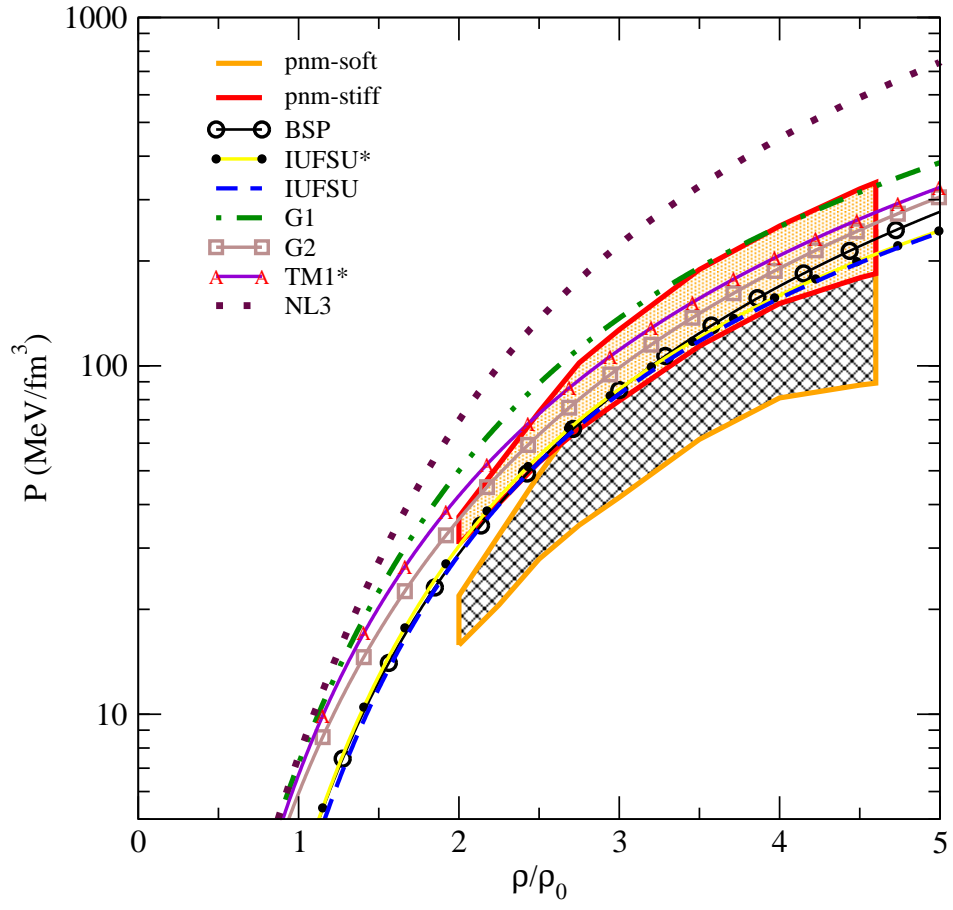


FIG. 5: (Color online) Same as Fig. 4, but, for the PNM.

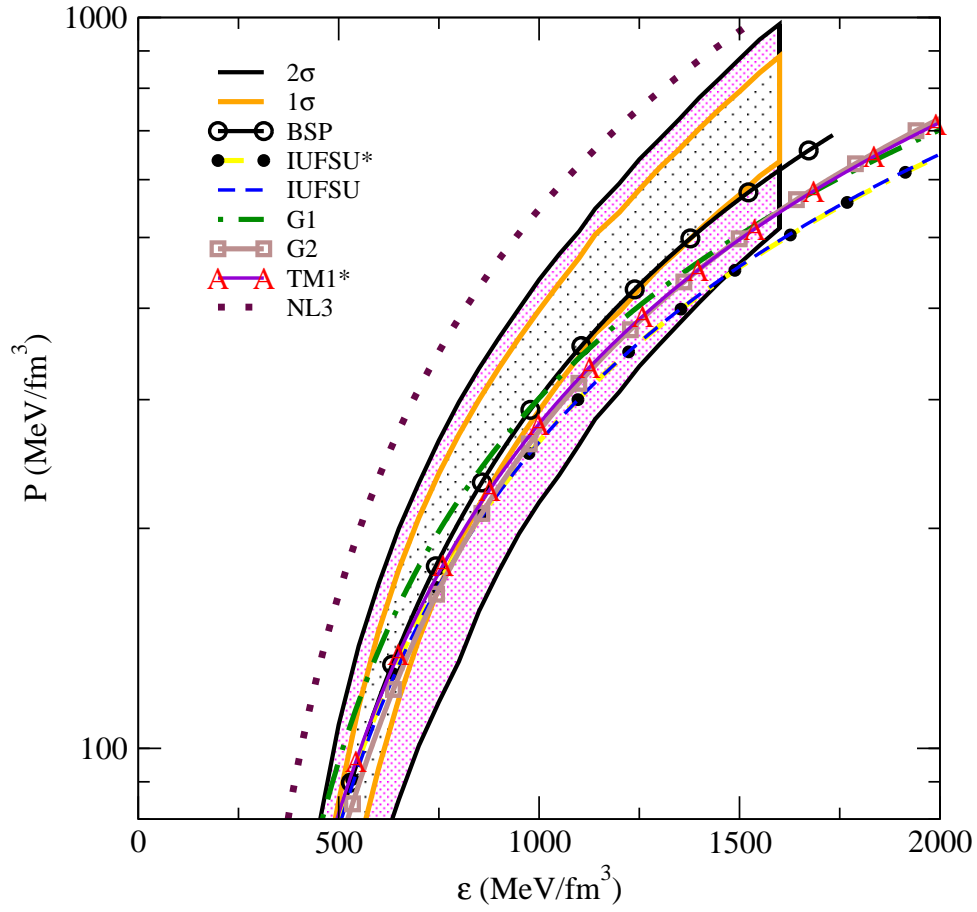


FIG. 6: (Color online) Pressure versus energy density for the beta equilibrated neutron rich matter. The shaded region represents the observational constraints taken from Ref. [33]. The orange and the black boundaries of the shaded regions are the EOSs within  $1\sigma$  and  $2\sigma$  limits, respectively.

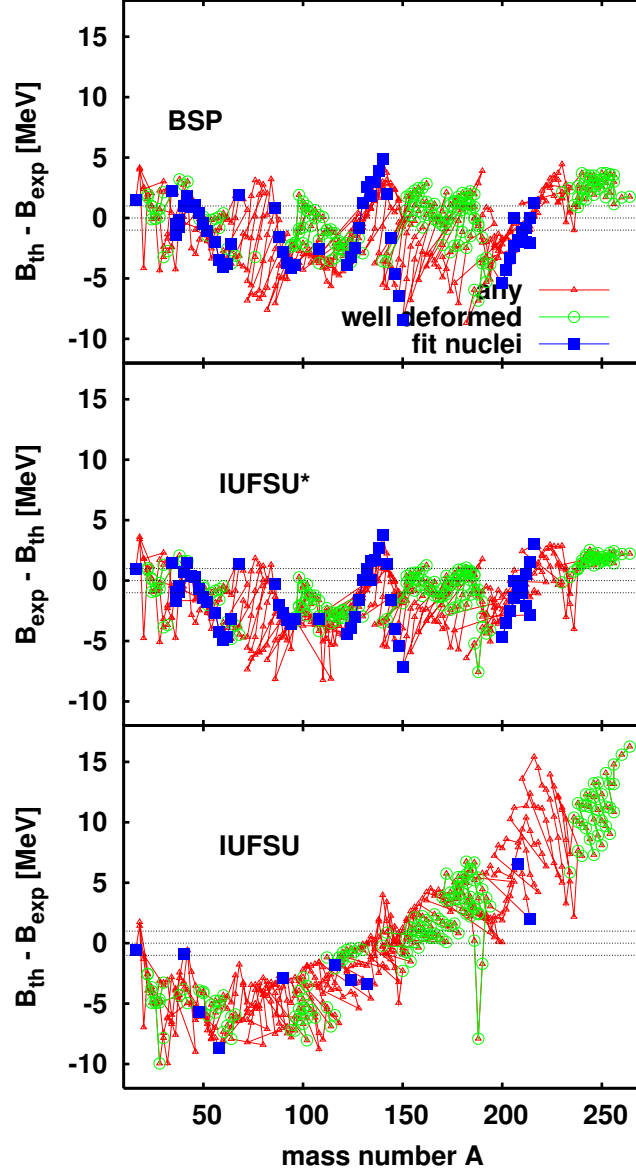


FIG. 7: (Color online) Binding energy systematics in terms of the errors  $\delta B$  (Eq. 18) as function of mass number  $A$  obtained for different parameterizations of the extended RMF model. The nuclei that were included in the fit are marked by filled squares, well-deformed nuclei by open circles, and all others by triangles. Binding energy error equal to zero and  $\pm 1$  MeV are indicated by faint horizontal lines. The corrections to the binding energies due to the pairing and quadrupole correlations are included for all the cases (see text for detail).

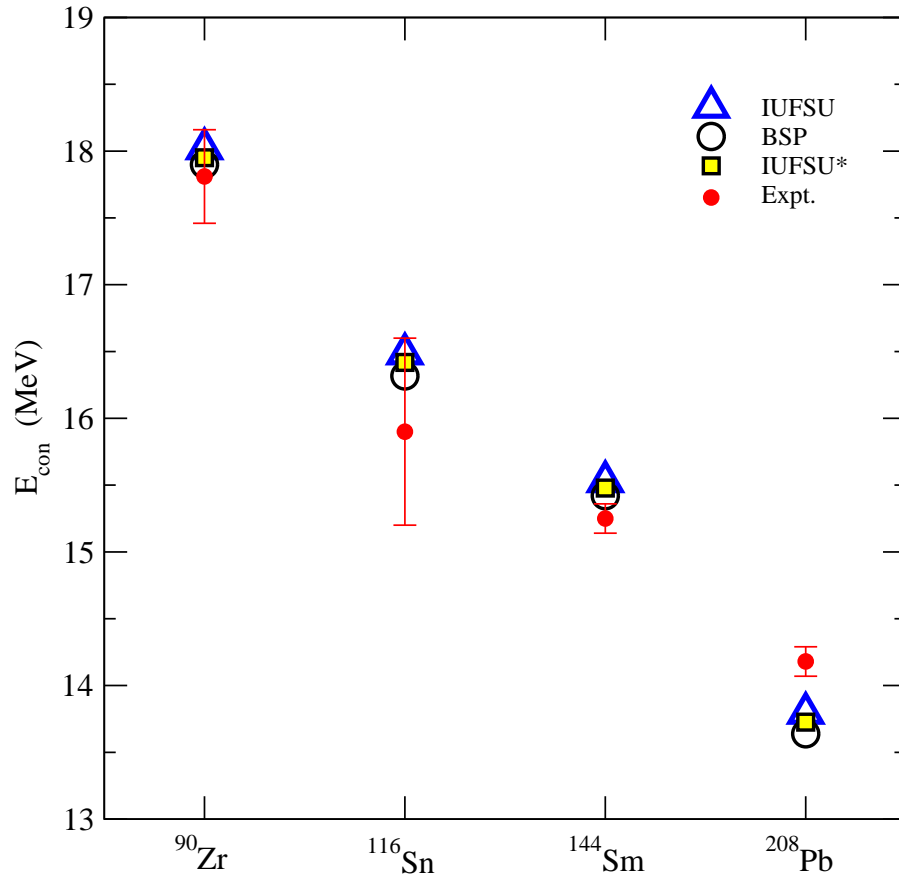


FIG. 8: (Color online) Fully self-consistent values for the constraint energy  $E_{\text{con}}$  (Eq. 19) of the iso-scalar giant monopole resonance are compared with the corresponding experimental data taken from Refs. [31].

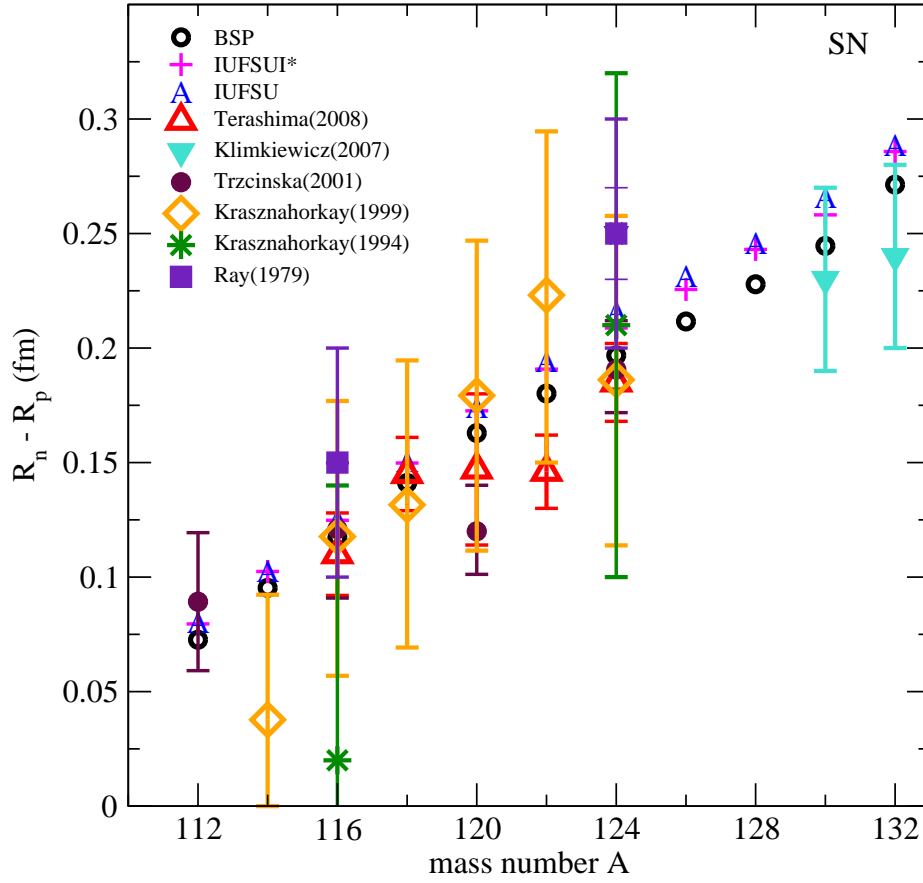


FIG. 9: (Color online) The neutron-skin thickness  $R_n - R_p$  for several tin isotopes for the BSP, IUFSU\* and IUFSU parameter sets. Experimental data are taken from Ref. [39, 43–47].

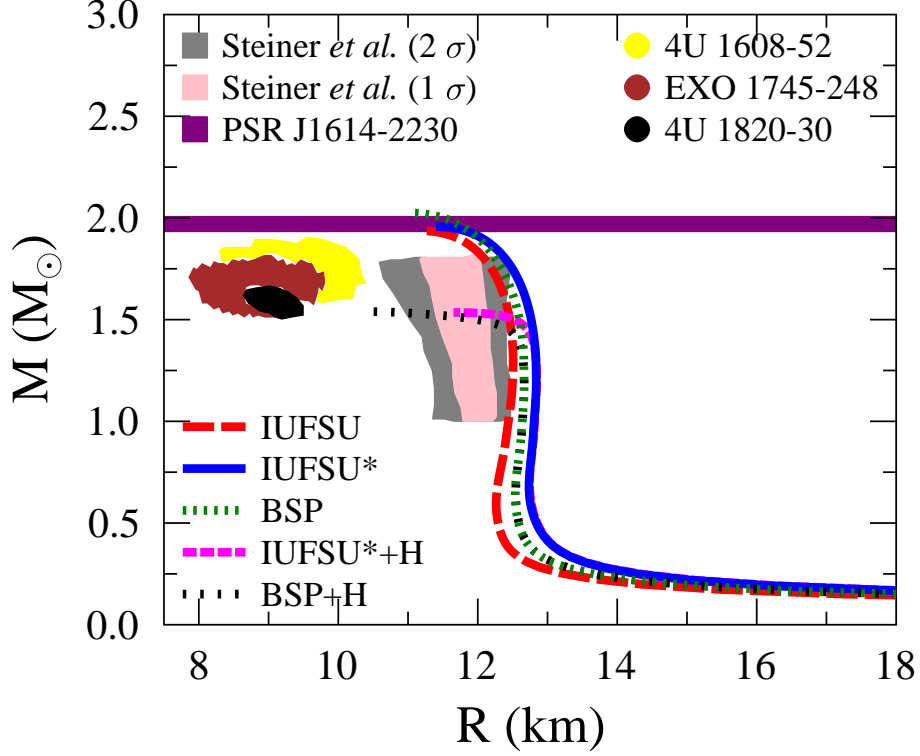


FIG. 10: (Color online) Mass-radius relation of BSP, IUFSU and IUFSU\* parameter sets using nucleonic EOS and hyperionic EOS. The observational three neutron data with  $1\sigma$  error bar that suggest small neutron star radii reported by Özel *et al.* in Ref. [55] as well as two shaded area that suggest larger radii with  $1\sigma$  and  $2\sigma$  error bars obtained by Steiner *et al.* ([33]). The horizontal shaded area is the mass of PSR J1614-2230 observation reported in Ref.[18].

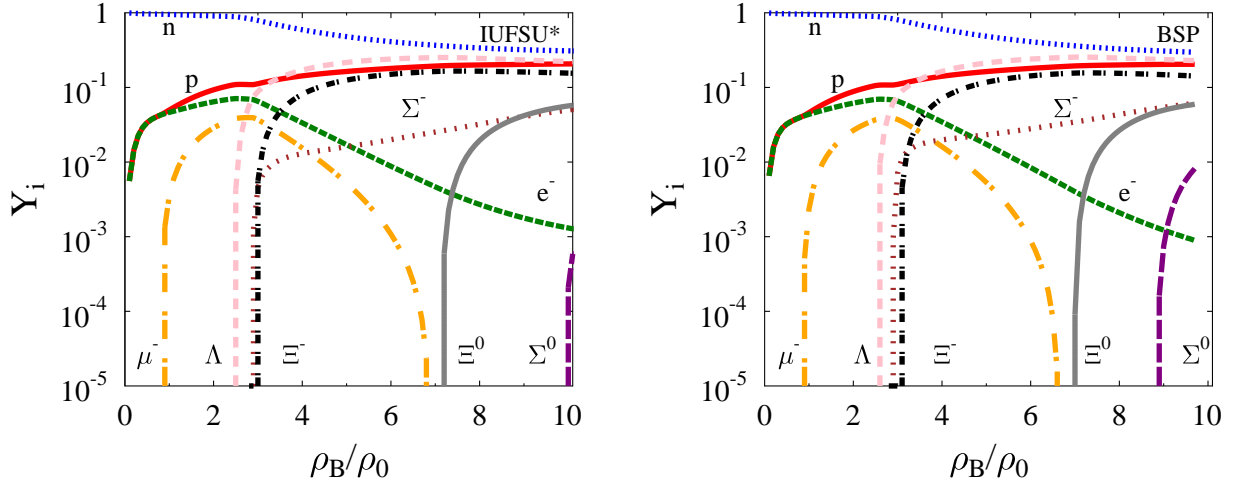


FIG. 11: (Color online) Particle fractions as a function of relative baryon density  $\rho_B/\rho_0$  for IUFSU\* and BSP parameter sets in the case hyperons are included.